Ultramicroscopy 217 (2020) 113069

Contents lists available at ScienceDirect

Ultramicroscopy

journal homepage: www.elsevier.com/locate/ultramic

Correction of EELS dispersion non-uniformities for improved chemical shift analysis

RWH Webster[a,*], AJ Craven[a], B Schaffer[b], S McFadzean[a], I MacLaren[a], DA MacLaren[a,*]

[a] SUPA, School of Physics & Astronomy, The University of Glasgow, Glasgow G12 8QQ, UK
[b] AMETEK GmbH, Ingolstädterstr. 12, 80807 Munich, Germany

ARTICLE INFO

Keywords:
Electron microscopy
Electron energy-loss spectroscopy
Post-column spectrometer
Spectrum imaging
Dispersion calibration

ABSTRACT

We outline a simple routine to correct for non-uniformities in the energy dispersion of a post-column electron energy-loss spectrometer for use in scanning transmission electron microscopy. We directly measure the dispersion and its variations by sweeping a spectral feature across the full camera to produce a calibration that can be used to linearize datasets post-acquisition, without the need for reference materials. The improvements are illustrated using core excitation electron energy-loss spectroscopy (EELS) spectra collected from NiO and diamond samples. The calibration is rapid and will be of use in all EELS analysis, particularly in assessments of the chemical states of materials via the chemical shift of core-loss excitations.

Introduction

Electron energy-loss spectroscopy (EELS) unlocks a wealth of information in the transmission electron microscope [1], providing spatially resolved measurements of compositional [2], plasmonic [3] and now even vibrational [4] properties of materials right down to the atomic scale. A number of improvements to spectrometer design [5–9] and control (e.g. [10–13]) have eased the acquisition and analysis of EELS datasets, substantially increasing the technique's popularity.

In addition to a spatial resolution that can resolve individual atoms, a clear advantage of EELS is that observation of the fine structure of energy-loss features can yield chemically-specific insight including the local bonding geometry and oxidation states of elements. For example, the positions of core-loss $L_{2,3}$ 'white lines' of *3d* transition metals shift to higher energies with increasing oxidation states, reflecting an increase in the binding energy of the core electronic state. Broadly, the $L_{2,3}$ edges of Cr [14], Mn, V and Fe [15] all shift of order 1 eV per increment of formal oxidation charge, with similar scaling for the edges of heavier metals [16], including Nb, [17], Ce [18] and, to a lesser extent, Mo [19]. With improved coupling of the specimen to the spectrometer [20], access to such edges has improved [16].

EELS edge position is also sensitive to the chemical nature of a bonded ligand [14], effectively through variations in the unoccupied density of states and changes in the multiplet structure that derive from the bonding environment. Greater shifts can be observed for the edges of polyvalent anions, notably the O K-edge in transition metal oxides (e.g. [15, 21]). However, such measurements are generally made relative rather than absolute in energy, and published edge positions can vary by over 2 eV [14, 22]. It is therefore common to use the separation of two features within a single spectrum as an alternative characteristic measurement that does not require absolute calibration, for example, the O K-edge and L_{23} edges of a 3d transition metal [21-23].

Accurate, absolute measurements in EELS require comparisons with well-characterised, stable reference materials under identical spectrometer conditions [7, 15, 24], which can be arduous. Ideally, we estimate that an accuracy of order 0.1 eV is desirable if chemical shifts in compounds with mixed valence states are to be analysed. Absolute calibration of the energy scale and dispersion of spectra is not standard practice because they are well-known to be susceptible to time-dependent environmental factors including ambient electromagnetic and thermal conditions, hysteresis in the magnetic electron-optical elements within the spectrometer, variations in the microscope alignment and even the positioning of ferromagnetic materials in the laboratory [7, 12, 13, 25, 26].

A further, often-overlooked complexity in the use of post-column spectrometers is that the dispersion of the electron beam through a magnetic prism and onto the detector is inherently non-linear and that, even with correction, residual aberrations can limit the absolute energy calibration to a few electron-volts [24]. Practically, this leads to a problem in comparing datasets collected under different acquisition conditions, even on the same microscope. In this work, we present a method which facilitates the measurement, characterisation and

* Corresponding author.
E-mail addresses: rwebster@physics.org (R. Webster), dmaclaren@physics.org (D. MacLaren).

https://doi.org/10.1016/j.ultramic.2020.113069
Received 3 March 2020; Received in revised form 26 June 2020; Accepted 29 June 2020
Available online 02 July 2020

correction of such dispersion non-uniformities. Our main focus is to increase the reliability of absolute energy-loss calibration to facilitate analysis of chemical shifts but the methodology can also be applied more generally, including the correction of dispersion non-uniformities prior to splicing together low loss and high loss spectra for Fourier-log deconvolution processing [27].

High resolution EELS spectra are commonly collected during scanning transmission electron microscopy (STEM), whereby a focused, near-monochromatic electron probe is rastered across a thin sample. At each probe position, a fraction of the transmitted electron beam loses energy to excitation processes within the sample – including excitation of plasmons, core-electron ionisation and photon production – and these signals can be analysed, pixel by pixel, in what is known as the Spectrum Imaging methodology [10, 11]. A spectrometer positioned at the end of the microscope ('post-column') is commonly used to collect the transmitted, now polychromatic electron beam and disperse it in energy by passing it through the perpendicular magnetic field of a sector magnet (or 'prism'), typically bending it through ninety degrees. Subsequent lenses are then used to magnify the dispersion [6], correct for optical aberrations and transfer the spectrum to a planar camera [8, 9].

Inherent to the Lorentz force on the electrons traversing the prism is that their radii of curvature, and hence dispersion, depend on both electron energy and the prism magnetic induction and do not produce a spectrum that is linear in energy at the dispersion plane (see Supplementary Information for a simple model). Modern post-column spectrometers [8, 9] therefore exploit the optical elements after the prism to linearize the spectra, with a typical 0.2% tolerance on the dispersion across a field of view that can subtend a 2 keV range of energy loss [9]. Deviations from the ideally uniform dispersion are known to be non-linear [24] so that the error in measured energy depends on the position of a feature on the detector; in addition, even small variations in dispersion – a differential term – can accumulate to account for significant errors in energy measurement across a scale of a few 100 eV. Thus, whilst it is common to calibrate with respect to one channel of the detector, measurements spanning a substantial portion of the detector can be compromised, including, for example, assessment of extended energy loss fine structure (EXELFS) [28], splicing of spectra [27] or the separation of core-loss peaks described above. It is these measurements that we aim to improve in software, post-acquisition.

After spectrometer alignment at a chosen dispersion, a user has three main controls over the portion of the energy loss spectrum subtended by the detector. The first is the magnetic induction, B, in the prism, which is controlled via the current through the sector magnet windings. Changes to B are relatively slow to settle (of order 100 ms, see Supplementary Information) and are susceptible to hysteresis effects; they are therefore not normally employed dynamically during rapid data acquisition but are routinely used to trim the position of the dispersed electron beam at the start of an experiment. As explored below, a complication in adjusting the prism is that it will also adjust the dispersion, which is undesirable because a modest change in prism current will alter the dispersion from its nominal calibration.

The second control of spectrum position is to adjust the primary beam energy, through modulation of the acceleration voltage of the electron microscope (commonly referred to as a High Tension, or HT, adjustment). An advantage of this method, exploited in energy filtered transmission electron microscopy (EFTEM) [1], is that the microscope's post-specimen lenses (including those of the spectrometer) can be aligned for a single electron energy that is then selected within the spectrometer by placing a slit in the dispersion plane. A disadvantage is that the beam becomes defocused at the sample plane as the beam energy is altered and must be manually corrected by refocusing the condenser lenses; it is also slow (also of order 100 ms, see Supplementary Information) and therefore inappropriate for dynamic, rapid acquisition within STEM spectrum imaging.

A third mechanism for control of spectrum position is to apply a positive potential to a tubular liner electrode within the prism. Electrons are thereby accelerated through the prism, then decelerated afterwards, and the technique has the advantage of leaving the rest of the electron optics unchanged [7]. Additionally, the low capacitance of this 'drift tube' electrode enables rapid switching, of order 10 microseconds, with little hysteresis, so that it can be adjusted dynamically and rapidly during spectral acquisition. Indeed, use of the drift tube underpins the 'DualEELS' methodology [5], whereby two regions of the energy loss spectrum can be acquired in rapid succession, simply by switching the drift tube voltage and, in modern spectrometers, simultaneously deflecting the beam onto a second dedicated portion of the detector camera [9]. In essence, the energy loss associated with the spectral range of interest is compensated by the energy increase set by the drift tube so that the recorded electrons in both spectra pass through the prism with the same energy and dispersion and are then recorded at the same channels of the detector. In practice, aberrations can arise because the drift tube can produce an electrostatic focusing effect for off-axis rays and because the electron energies of the two spectra will differ within the post-prism optics. Both effects are small and drift-tube focusing is generally compensated for during spectrometer alignment.

In combination with optimisation of the detector acquisition timings, DualEELS increases the effective dynamic range of the detector, so that both the intense elastically scattered 'zero loss peak' and weaker energy-loss features can be acquired with adequate signal to noise ratios [5]. This ability to rapidly switch between two spectral regions also underpins several detailed studies requiring absolute energy calibration [7, 15, 24], where the zero-loss peak is measured before and after acquisition of a spectral feature of interest, so that artefacts such as drift in the primary energy can be isolated. Implicit in such measurements is that the energy range of the spectral feature is relatively small and that the feature is positioned to span the same detector positions as the reference peak. In this way, the dispersion and any aberrations are the same for both measurements. We aim to extend this methodology by positioning a reference spectrum at multiple points across the detector and will discuss the optimal means of achieving the necessary spectral shifts.

Materials and methods

EELS experiments employed a JEOL ARM200CF probe-corrected TEM/STEM instrument operated at 200 kV and equipped with a cold field emission source. A Gatan 965 Quantum ER spectrometer [9] with DualEELS [5] capabilities (including fast shutter, high speed VSM and 2048 × 2048 pixel Ultrascan camera options) was used for recording spectra in spectroscopy mode (i.e. with the microscope configured for STEM imaging, with the spectrometer's object plane set to the projector lens crossover and with a diffraction disk on the viewing screen). A nominal 0.1 nm probe was used for the spectrum acquisition and the convergence and collection semi-angles for all EELS data were 29 mrad and 36 mrad, respectively, using a nominal 2 cm camera length and the 2.5 mm spectrometer entrance aperture.

EELS data were collected shortly after the spectrometer had been realigned to minimise the non-uniformity of the dispersion. The spectrometer camera was operated in the 'high quality' readout mode, typically employing 1 × 5 binning, recently-collected gain and dark reference corrections and pre-set dispersions as indicated in the results section.

Separate tests of the beam stability on the spectrometer camera indicated that the cumulative effects of beam instabilities and environmental factors resulted in an apparent drift in the primary beam energy of 0.07 eV/min, with peak to peak oscillations of 0.2 eV and characteristic frequencies indicative of nominal 50 Hz mains frequency (see Supplementary Information). Variations of this magnitude are likely to be present in the data and care was therefore taken to avoid acquisition timings in Dual EELS where the position of the beam in the two spectra appeared to oscillate out of phase. All acquisition and

processing was conducted within the Gatan Digital Micrograph software package (GMS 2.3) [29].

Two samples are analysed here. The first is a relatively thick NiO sample provided by Gatan and routinely used for spectrometer calibration. An advantage of using NiO is that reduction to Ni metal only shifts the L_3 peak position by -0.2 eV [24, 30-32] because the *d*-band electron occupation level for the final state of the electronic transition is largely unchanged. The second sample is an undamaged region of a single crystal diamond sample that has been discussed for other purposes previously [33] and that was chosen to produce a well-characterised, strong EELS edge with fine structure that enables rapid identification of beam damage.

Dispersion characterisation and correction

Non-uniformities in the energy dispersion were measured using a custom automated acquisition routine [34] written using the Digital Micrograph (DM) scripting language. It is similar in function to simpler scripts used for 'engineer alignment' of the spectrometer dispersion, a previous approach to energy calibration [35] and a recently-published protocol for 'energy offset correction' of spectra, which scans spectra through a small energy range in order to smooth-out fixed-pattern noise [36].

The microscope and spectrometer were first aligned without a sample so that a sharp, focused zero-loss peak (ZLP) was positioned at the 'zoom point', the 200th channel from the left (high energy) edge of the CCD camera. Fig. 1 outlines the subsequent process. The peak position was first adjusted to lie close to the right-hand edge of the camera (ie. lower energy, or high energy-loss) using either the prism adjust or by reducing the primary beam energy (hereafter referred to as 'HT adjust'), refocusing the beam using the microscope's condenser system in the latter case: we explore the consequences of both changes below. It was not necessary to refocus the spectrometer in either case, with typical defocusing of the ZLP across the spectrum being limited to at most two detector channels. Similarly, small adjustments to the microscope's condenser system were not observed to shift the ZLP on the detector.

The script operated by opening a background thread in DM that grabbed frames from the live view of the DualEELS spectrum acquisition. Following the HT or prism adjust, the drift tube was then used to incrementally shift the position of the ZLP across the detector, using the DualEELS methodology to alternate between the un-deflected ZLP (drift tube off, static position at right hand side of detector) and the deflected peak (drift tube on to increment the ZLP across the detector; see insets to Fig. 1). A 100 ms delay was introduced between steps to accommodate software overheads. This produced two Spectrum Images (SIs). The SI in the high loss channel contained the deflected ZLPs while that in the low loss channel contained the un-deflected ZLPs. Each is a 2-dimensional data set with axes of camera channel number and acquisition number, with each row representing one ZLP acquisition that appears as a single white spot in Fig. 1. Recording the un-deflected ZLP channel enables instabilities in the beam energy to be monitored and minimised, typically to 'jitter' of order 0.2 channels. The voltage applied to the drift tube can be compared directly to the measured ZLP peak position as its position was incremented across the camera to produce a mapping from detector channel number to energy. It is important to record the voltage applied to the drift tube (as reported by the software) rather than the values requested by the routine, since the latter are susceptible to rounding errors and the bit depth of the drift tube power supply. (A glitch is noticeable, for example, around 32 V when working at dispersions of 0.025 eV/channel and 0.01 eV/channel.) Typically, we incremented the drift tube voltage to move the ZLP ten channels each cycle, producing an SI containing over 200 individual spectra that took 2 min to acquire.

To measure the dispersion across the detector, each ZLP was fitted to determine its position to sub-pixel accuracy. The fidelity of position determination is not strongly dependent on the choice of fitting function so, for speed and simplicity, we applied a Gaussian fit to the centre of the ZLP profiles. We then determined the separation of the deflected and un-deflected ZLPs in order to determine the energy for each incremented low loss ZLP position. Using the difference between high loss and low loss peaks - rather than simply the incremented position of the ZLP - allowed jitter and drift to be monitored, since both peaks are affected similarly by energy instabilities. If substantial drift or jumps were observed in either peak, the measurement was repeated.

When using the HT offset, the ZLP was not brought back exactly to the zoom point when a compensating voltage of equal magnitude was applied to the drift tube: this is contrary to the ideal behaviour predicted by Eqn. 3 in the Supplementary Material. The error was approximately proportional to the offset applied and so a linear correction was applied in this case (see Supplementary Information). A fifth order polynomial was then fitted to the positions as a function of energy, so that the data could be re-sampled onto a linear energy scale by cubic polynomial interpolation [37], taking care to redistribute the intensity between channels in accordance with their non-linear sampling [38]. We conducted this procedure each time the spectrometer dispersion was changed and at the start of each acquisition session.

Results and discussion

In Fig. 2, the measured effects of dispersion non-uniformities are presented for several nominal dispersion alignments. The data are presented as channel-by-channel differences in measured energy compared to the nominal alignment, so that a linear trend indicates a uniform difference in the dispersion across the camera. The data are all aligned with respect to the zoom point, where the ZLP is usually positioned during SI acquisition. Calibration scans are presented for both the HT adjust (Fig. 2a) and prism adjust (Fig. 2b) approaches. The average of the residuals after subtraction of a best-fit polynomial are plotted in Fig. 2c. The average is over all dispersions and gives a non-zero mean suggesting that there is a contribution from the camera itself while the standard deviations are indicative of jitter and instabilities in the beam position.

Two main observations can be made of Fig. 2. First, there are substantial variations in the measured energy across the detector that are of a similar high-order polynomial form to those noted previously [24]. For the 1 eV/channel and 0.5 eV/channel settings in particular, these variations correspond to errors in energy measurement of several electron volts that would complicate high resolution analysis of chemical shifts. Furthermore, we find that the details of these errors can drift from day to day and will occasionally undergo larger, apparently unpredictable variations that may be related to changes in the spectrometer environment: their rapid assessment as part of standard operating procedures is therefore desirable. It is also worth noting that any significant prism adjustment, for example, to 're-centre' the ZLP during tuning, will also cause variations in the measured calibration.

A second, striking observation of Fig. 2 is the clear difference in the energy errors between the two modes of measurement: whilst the average dispersions measured using an initial prism adjust agree with their nominal values, those measured using an initial HT adjustment are systematically smaller than the nominal settings. The difference between the two measurements is a natural consequence of them being taken with a different prism setting, since the prism current alters the dispersion as well as the ZLP position. Since the data collected with an initial HT offset use the same prism setting as that of a real SI measurement, this is our preferred methodology. However, a good approximation to the linear difference between 'HT adjust' and 'prism adjust' can be calculated by consideration of the Lorentz force acting on the electrons passing through the spectrometer (see Supplementary Information). This correction may be useful for correcting energy loss datasets that extend beyond the range of the drift-tube power supply, where a prism offset must be used, such as analysis of edges beyond an

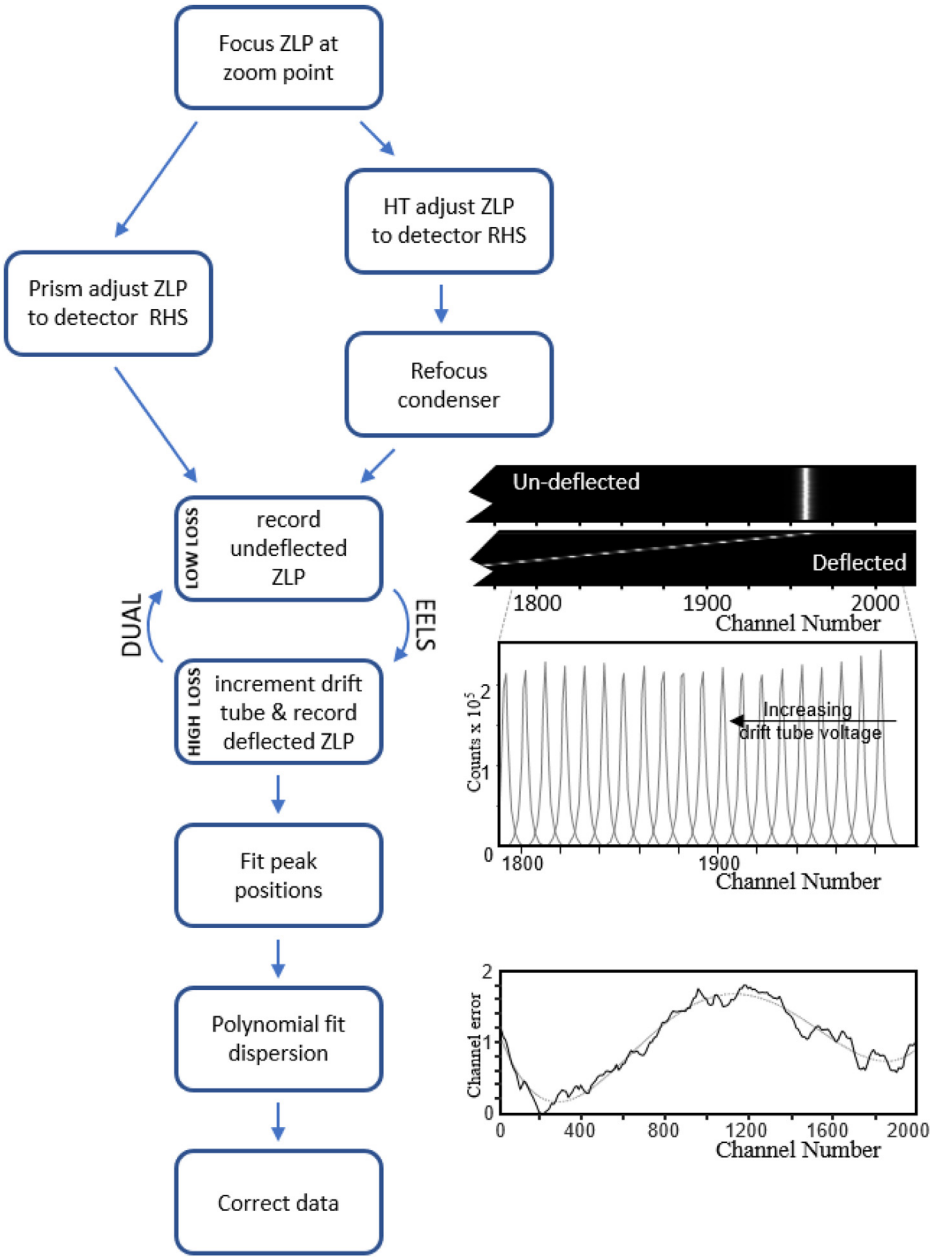

Fig. 1. Flow diagram outlining the process for measuring and removing dispersion non- uniformities. After shifting the ZLP to the right of the spectrum using either the magnetic sector ('prism adjust') or a change in the primary beam energy ('HT adjust'), the drift tube is used to increment the energy to produce a Dual EELS data set with a fixed 'low loss' ZLP position (inset, upper spectrum image, labelled 'un-deflected') and a series of displaced ZLPs in the 'high loss' spectrum image (inset, lower spectrum image, labelled 'deflected' and with detail of individual peaks shown below). The peak positions are determined and the trends fitted with a 5th order polynomial (lower panel) that can be used to correct subsequent EELS data sets with sub-pixel precision.

energy loss of 3 keV [16].

The order of the polynomial used to fit the non-uniformities is arbitrary but 5th order was found to be a good approximation to the trends observed in Fig. 2. We justify the use of a low-order polynomial on the basis that electron-optical aberrations and their correction in the spectrometer are anticipated to be smoothly-varying across the field of view. Such a fit does not, however, eliminate the higher frequency variations that are also evident. (See, for example, the pronounced dips in the 1 eV/channel dataset of Fig. 2(b)). Since these variations are similar for all the measured dispersions, we attribute them to the detector and the same fixed-pattern variations that have been addressed by energy offset correction routines previously [13, 36]. They likely derive from the physical construction of the detector's fibre-optic array and pixelated CCD camera, which causes a slight, non-uniform redistribution of counts between channels; the nature of the redistribution is intensity-dependent and so cannot be eliminated with improved gain references alone. Ultimately, these small variations limit the precision to which the position of an energy loss feature can be determined since they contain similar spatial frequencies to the loss features themselves; for example, co-incidence of a dip in this fixed-pattern error with the onset of an EELS edge will shift slightly the apparent edge position. The problem has been discussed in detail in earlier reports and can be reduced by averaging energy-shifted spectra [13, 36].

We now turn to the application of the correction algorithm to experimental data. Figs. 3 and 4 show the improved alignment of energy loss features that have been collected under a number of spectrometer settings. Fig. 3 shows the $L_{2,3}$ core-loss edge of a NiO sample after removal of plural scattering by Fourier ratio deconvolution of the low-loss signal; this was chosen since it is used as a reference material for spectrometer alignment. The energy of the L_3 peak is commonly taken to be 852.75 eV [1], although the literature contains a spread of experimental results about this value [14, 22, 24, 31, 32], and the spectrometer was originally aligned by the engineer to place the L_3 peak at 853.0 eV, all of which illustrate the difficulty in making absolute energy-loss measurements. Fig. 3(a) presents the same EELS feature, collected under a range of dispersion and drift-tube settings, replicating the types of variations in acquisition conditions that are made during typical experiments (for example, the EELS edges that need to be

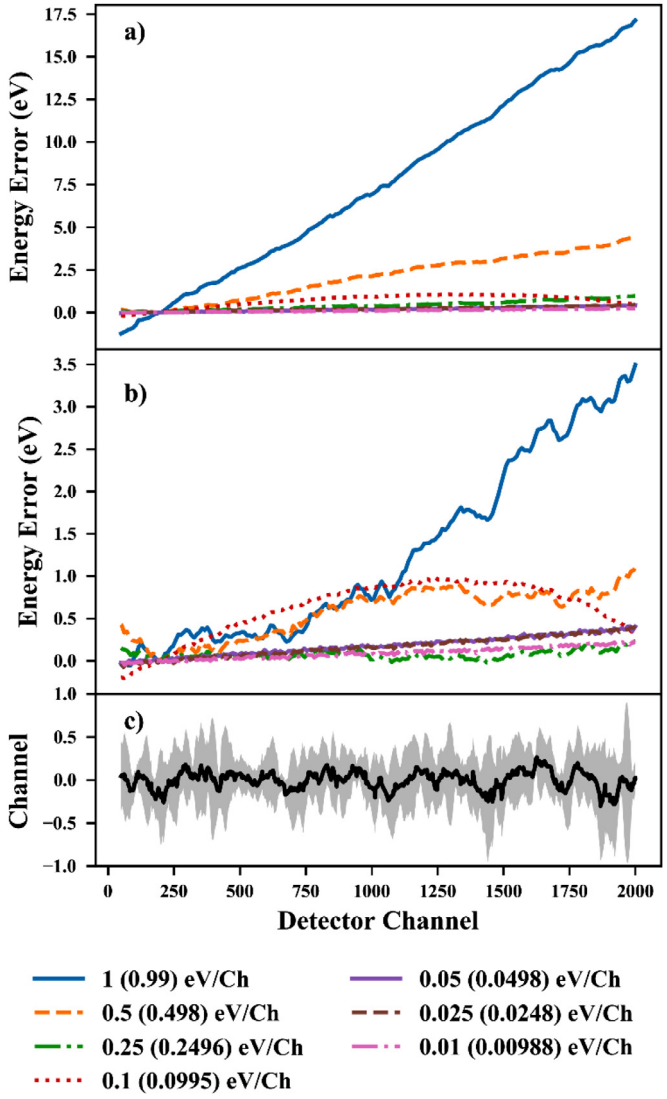

Fig. 2. Measured effects of dispersion deviations for each of the nominal dispersion settings measured by starting with (a) an offset in the primary beam voltage (HT offset) and (b) an offset in the prism adjust, with (c) the mean (black line) and standard deviation (shaded region) of the residuals of polynomial fits for all dispersions (HT offset). In each case the measured mean dispersion (using the HT offset) is indicated in brackets in the legend and typically differs from the nominal value by less than 1%. Note that the data in the upper panel (a) deviate from the nominal dispersion with a linear trend that can produce an absolute error of several electron volts at the right of the spectra: this is notable because it reflects the conditions of a real experiment.

collected simultaneously determine the dispersion and the energy offset required and hence the drift tube voltage). These data sets were collected using the 'HT adjust' protocol outlined in Fig. 1.

Without correction, the energy of the $L_{2,3}$ peaks in Fig. 3a appears to vary by ~5 eV, depending on where it has been placed on the camera, and on the dispersion, in accordance with the trends illustrated in Fig. 2(a). The lower panel, Fig. 3(b) shows the same spectra after dispersion correction, where the $L_{2,3}$ peaks now align to within 0.1 eV. It is important to note that the peaks have not simply been shifted in a relative sense (for example, using the DM 'peak align' tool) but have been recalibrated onto an absolute energy-loss scale using the correction algorithm outlined in Fig. 1. The mean peak position of 852.9 eV is in excellent agreement with the calibration of the drift tube voltage, and therefore, with the expected peak energy of 852.75 eV.

A similar improvement in energy measurement is shown in Fig. 4, which presents the aligned carbon K-edge measured from crystalline diamond under several spectrometer conditions and again after deconvolution of plural scattering (see Supplementary Information). As outlined previously [39, 40], the K-edge EELS spectrum of diamond is dominated by a sharp exciton peak at 289 eV, followed by features of oscillating intensity that derive from excitation to overlapping σ* states, the nature of the bandgap and multiple scattering EXELFS features that can be used to measure crystallographic spacing. Absent from the spectra is a pre-edge feature that indicates the existence of sp^2-bonded carbon and hence beam damage [33]. The spectra are again aligned to better than a single channel in each case and typically within 0.1 eV. There is also good alignment of all the spectral features extending beyond the edge onset, which is important for accurate measurement of EXELFS effects (and is also important for accurate splicing of spectra for Fourier-log deconvolution [27]). There is clearly a variation in peak broadening that corresponds to the difference in resolution at different dispersion settings and the alignment of features here makes feasible experiments where EELS edges are acquired under different spectrometer conditions while retaining energy calibration.

We turn, finally, to the precision to which the energies of EELS features can be measured and identify two main limitations that the spectrometer operator should be aware of and, ideally, would characterise. The first is the accuracy and calibration of the power supplies used for the HT offset and drift tube. For example, aligning the spectra of Fig. 3 to within 0.1 eV requires an accuracy of order 0.01%, which is reasonable for modern precision equipment. However, we caution that neither power supply should be considered to be calibrated absolutely since both can be adjusted during spectrometer alignment. A simple check for the HT offset is to ensure that it can be used to place a well-known energy loss feature, such as those of the samples described here, at the zoom point. An advantage of this measurement is the equivalence of the absolute electron energies of (i) the ZLP prior to HT offset and (ii) the chosen energy loss feature after the HT offset is applied. This equivalence ensures that the trajectories of the two beams are identical through all the post-specimen optics including the spectrometer, so that the effect of a change in beam energy can be isolated. In contrast, it is difficult to isolate the calibration of the drift tube from the optimisation of post-prism chromatic aberrations, the latter of which will differ for the two spectra in a Dual EELS dataset. Indeed, because the drift tube calibration is trimmed during spectrometer alignment, its accuracy will be subject to a trade-off with the wider constraints of minimising aberrations in the complex post-prism optics. As a consequence, we find that applying an HT offset and compensating with a nominally-identical drift tube voltage produces a slight shift in spectral position that must be corrected. The alignment of spectra in Figs. 3 and 4 is ultimately limited by the precision of such a correction, and here we achieve alignment to within 0.1 eV. It would be feasible to improve the accuracy of our methodology by incorporating a sweep of the HT offset to calibrate the drift tube (incorporating post-prism aberrations): this would be slowed by the need for dynamic refocusing of the condenser but such calibration would not need to be applied on a daily basis.

A second, separate consideration is the long-term drift of the measured ZLP, which here we estimate to be 0.07 eV/min. In principle, our routines will correct for any drift in absolute beam energy, since they effectively calibrate positions on the detector directly and a drift in absolute beam energy will produce a shift in ZLP position that can also be measured. However, some of the measured drift is expected to arise from thermal or relaxation effects in the prism, which subtly alter the magnetic induction experienced by the beam: these cannot be removed by the routine and errors are expected to accumulate with time. Thus, the routine outlined in Fig. 1 is best run immediately before or after critical measurements. Such an approach will also help to eliminate the effect of environmental factors, which can be difficult to predict. Within these limitations, we are able to align spectral features to within 0.1 eV using the routines described here. This is a substantial improvement on our existing spectrometer alignments, which we have shown can lead to

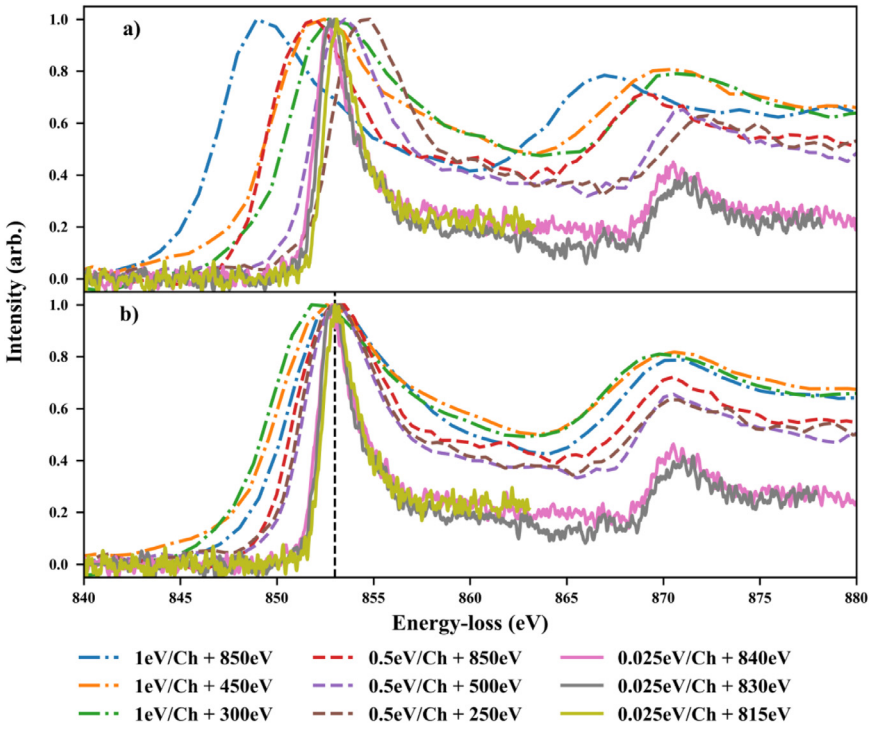

Fig. 3. Comparison of the (a) as-collected and (b) dispersion-corrected (using the 'HT adjust' protocol) core-loss EELS measurements of the Ni $L_{2,3}$ edges of NiO recorded using a range of drift-tube voltages and dispersions (indicated in the legend). Correction leads to alignment of spectra to within 0.1 eV with a mean peak position of 852.9 eV. Intensities are normalised to the Ni L_3 peak maximum.

errors of several electron volts in the worst cases.

Conclusions

We have demonstrated an improved methodology for measurement of the absolute energy of electron energy loss features that extend across a significant fraction of the detector. It is a logical extension of previous use of DualEELS to directly calibrate a single energy channel in a spectrum and removes the need for inconvenient reference materials that can, as shown here, be compromised by beam damage effects. By effectively calibrating the detector at a range of electron energies, the fidelity of energy calibration is improved across the entire measured spectrum. The algorithm will be of use for EELS measurements that extend across several hundred electron volts in energy, including accurate measurements of extended fine structure and of the separation of distinct EELS edges, used for assessment of a material's chemical identity including oxidation and bonding states.

Declaration of Competing Interest

None.

Acknowledgements

We are grateful for the DM scripts and discussion shared by Dr. Wang [36] and also for discussions with Prof. Phil Batson and Dr. Bernd Krauss. Aspects of the work were funded by the Engineering and Physical Sciences Research Council of the UK through grants EP/N017218/

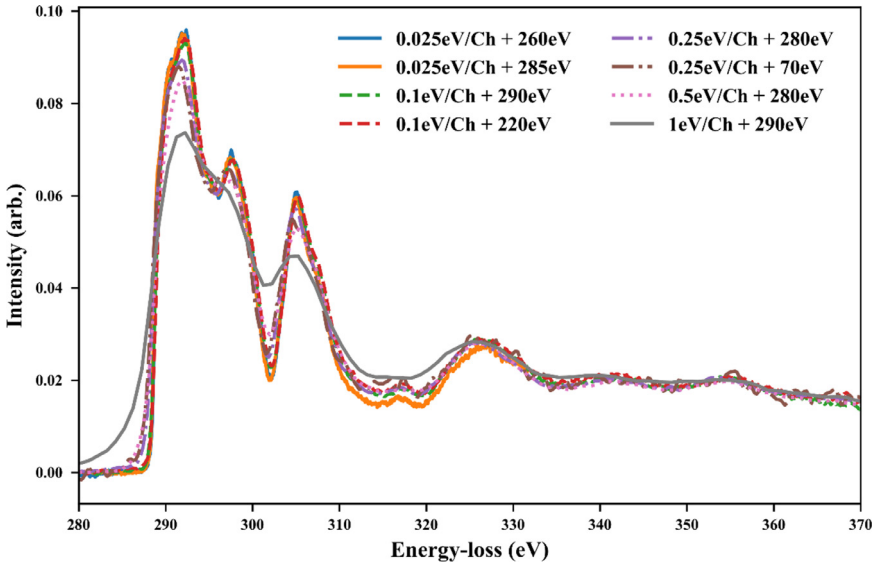

Fig. 4. Dispersion-corrected carbon K-edge core-loss EELS measurements of diamond collected under a range of dispersions and drift-tube voltages, as indicated in the legend. Spectra are normalised by intensity between 285 and 305 eV. The 'HT adjust' protocol was applied to improve the dispersion.

01 and EP/N509668/1 and the instrumentation was funded by the University of Glasgow and Scottish Universities Physics Alliance.

Supplementary materials

Supplementary material associated with this article can be found, in the online version, at doi:10.1016/j.ultramic.2020.113069. Research data and scripts are available at doi:10.5525/gla.researchdata.1032.

References

[1] R.F. Egerton, Electron Energy Loss Spectroscopy in the Electron Microscope, Springer, 2011.
[2] R.F. Egerton, Electron energy-loss spectroscopy in the TEM, Rep. Prog. Phys. 72 (2009) 016502.
[3] O. Nicoletti, F. de la Peña, R.K. Leary, D.J. Holland, C. Ducati, P.A. Midgley, Three-dimensional imaging of localized surface plasmon resonances of metal nanoparticles, Nature 502 (2013) 80.
[4] O.L. Krivanek, T.C. Lovejoy, N. Dellby, T. Aoki, R.W. Carpenter, P. Rez, E. Soignard, J. Zhu, P.E. Batson, M.J. Lagos, R.F. Egerton, P.A. Crozier, Vibrational spectroscopy in the electron microscope, Nature 514 (2014) 209.
[5] J. Scott, P.J. Thomas, M. MacKenzie, S. McFadzean, J. Wilbrink, A.J. Craven, W.A.P. Nicholson, Near-simultaneous dual energy range EELS spectrum imaging, Ultramicroscopy 108 (2008) 1586.
[6] T. Oikawa, N. Shibata, K. Nakanishi, Y. Kokubo, Y. Bando, An EELS spectrometer with a double dispersion lens for a medium voltage TEM, J. Electron Microsc. 35 (1986) 353.
[7] P.E. Batson, S.J. Pennycook, L.G.P. Jones, A new technique for the scanning and absolute calibration of electron energy loss spectra, Ultramicroscopy 6 (1980) 287.
[8] A.J. Gubbens O. L. Krivanek, N. Dellby, Developments in EELS instrumentation for spectroscopy and imaging, Microsc. Microanal. Microstruct. 2 (1991) 315.
[9] A. Gubbens, M. Barfels, C. Trevor, R. Twesten, P. Mooney, P. Thomas, N. Menon, B. Kraus, C. Mao, B. McGinn, The GIF Quantum, a next generation post-column imaging energy filter, Ultramicroscopy 110 (2010) 962.
[10] C. Jeanguillaume, C. Colliex, Spectrum-image: the next step in EELS digital acquisition and processing, Ultramicroscopy 28 (1989) 252.
[11] J.A. Hunt, D.B. Williams, Electron energy-loss spectrum-imaging, Ultramicroscopy 108 (1991) 1586.
[12] D.R.G. Mitchell, B. Schaffer, Scripting-customised microscopy tools for Digital Micrograph, Ultramicroscopy 103 (2005) 319.
[13] M. Bosman, V.J. Keast, Optimizing EELS acquisition, Ultramicroscopy 108 (2008) 837.
[14] T.L. Daulton, B.J. Little, Determination of chromium valence over the range Cr(0)-Cr(VI) by electron energy loss spectroscopy, Ultramicroscopy 106 (2006) 561.
[15] H. Tan, J. Verbeeck, A. Abakumov, G. Van Tendeloo, Oxidation state and chemical shift investigation in transition metal oxides by EELS, Ultramicroscopy 116 (2012) 24.
[16] I. MacLaren, K.J. Annand, C. Black, A.J. Craven, EELS at very high energy losses, Microscopy 67 (2018) i78.
[17] D. Bach, R. Schneider, D. Gerthsen, J. Verbeeck, W. Sigle, EELS of Niobium and Stoichiometric Niobium-Oxide Phases - Part I: Plasmon and Near-Edges Fine Structure, Microsc. Microanal. 15 (2009) 505.
[18] L.A.J. Garvie, H. Xub, Y. Wang, R.L. Putnam, Synthesis of $(Ca,Ce_3C,Ce_4C)_2Ti_2O_7$: a pyrochlore with mixed-valence cerium, J. Phys. Chem. Solids 66 (2005) 902.
[19] L. Lajaunie, F. Boucher, R. Dessapt, P. Moreau, Quantitative use of electron energy-loss spectroscopy Mo-$M_{2,3}$ edges for the study of molybdenum oxides, Ultramicroscopy 149 (2015) 1.
[20] A.J. Craven, H. Sawada, S. McFadzean, I. MacLaren, Getting the most out of a post-column EELS spectrometer on a TEM/STEM by optimising the optical coupling, Ultramicroscopy 180 (2017) 66.
[21] L. Yedra, E. Xuriguera, M. Estrader, A. López-Ortega, M.D. Baró, J. Nogués, M. Roldan, M. Varela, S. Estradé, F. Peiró, Oxide wizard: an EELS application to characterize the white lines of transition metal edges, Microsc. Microanal. 20 (2014) 698.
[22] H.K. Schmid, W. Mader, Oxidation states of Mn and Fe in various compound oxide systems, Micron 37 (2006) 426.
[23] T. Riedl, T. Gemming, W. Gruner, J. Acker, K. Wetzig, Determination of manganese valency in $La1_xSr_xMnO_3$ using ELNES in the (S)TEM, Micron 38 (2007) 224.
[24] P.L. Potapov, D. Schryvers, Measuring the absolute position of EELS ionisation edges in a TEM, Ultramicroscopy 99 (2004) 73.
[25] Y. Sasano, S. Muto, Energy-drift correction of electron energy-loss spectra from prolonged data accumulation of low SNR signals, J. Electron Microscopy 57 (2008) 149.
[26] K. Kimoto, Y. Matsui, Software techniques for EELS to realize about 0.3eV energy resolution using 300kV FEG-TEM, J. Microscopy 208 (2002) 224.
[27] A. Craven, B. Sala, I. MacLaren, EELS analysis of nano-sized particles in a matrix, Microscopy & Microanalysis 24 (2018) 436–437, https://doi.org/10.1017/S1431927618002672.
[28] M. Sarikaya, M. Qian, E.A. Stern, EXELFS Revisited, Micron 27 (1996) 449.
[29] http://www.gatan.com/products/tem-analysis/gatan-microscopy-suite-software, accessed May 2019.
[30] R.D. Leapman, L.A. Grunes, P.L. Fejes, Study of the $L_{2,3}$ edges in 3d transition metals and their oxides by electron energy-loss spectroscopy with comparisons with theory, Phys. Rev. B 26 (1985) 614.
[31] J. Fink, Th. Muller-Heinzerling, W.Speier B.Scheerer, F.U. Hillebrecht, J.C. Fuggle, J. Zaanen, G.A. Sawatzky, 2p absorption spectra of the 3d elements, Phys. Rev. B 32 (1985) 4899.
[32] J.C. Fuggle, N. Martensson, Core-level binding energies in metals, J. Electron Spect. Rel. Phenom. 21 (1980) 275.
[33] P.S. Salter, M.J. Booth, A. Courvoisier, D.A.J. Moran, D.A. MacLaren, High resolution structural characterisation of laser-induced defect clusters inside diamond, Appl. Phys. Lett. 111 (2017) 081103.
[34] Scripts available at http://dx.doi.org/10.5525/gla.researchdata.1032.
[35] C.E. Meyer, C.B. Boothroyd, A.J. Gubbens, O.L. Krivanek, Measurement of TEM primary energy with an electron energy-loss spectrometer, Ultramicroscopy 59 (1995) 283.
[36] Y. Wang, M.R.S. Huang, U. Salzberger, K. Hahn, W. Sigle, P.A. van Aken, Towards atomically resolved EELS elemental and fine structure mapping via multi-frame and energy-offset correction spectroscopy, Ultramicroscopy 184 (2018) 98.
[37] J. Mooney, P. Kambhampati, Get the basics right: jacobian conversion of wavelength and energy scales for quantitative analysis of emission spectra, J. Phys. Chem. Lett. 4 (2013) 3316.
[38] William H. Press, Saul A. Teukolsky, William T Vetterlin, Numerical Recipes 3rd Edition: The Art of Scientific Computing, 3rd edition, Cambridge University Press, New York, NY, USA, 2007.
[39] L.A.J. Garvie, P.R. Busek, A.J. Craven, Electron-loss near-edge structure (ELNES) as a probe of valence and co-ordination number, Can. Mineral. 33 (1995) 1157.
[40] F.L. Coffman, R. Cao, P.A. Pianetta, S. Kappor, M. Kelly, and L.J. Terminello. Near-edge x-ray absorption of carbon materials for determining bond hybridization in mixed sp2/sp3 bonded materials. 69, 69:568, 1996.